**Periodica Polytechnica Civil Engineering**, 69(2), pp. 644–663, 2025

# Determination of Rail Dilatation Movements at Tunnel Gates for Ballasted Railway Tracks

Nándor Liegner[1]*

[1] Department of Highway and Railway Engineering, Faculty of Civil Engineering, Budapest University of Technology and Economics, Műegyetem rkp. 3., H-1111 Budapest, Hungary
* Corresponding author, e-mail: liegner.nandor@emk.bme.hu

Received: 31 July 2024, Accepted: 02 February 2025, Published online: 04 March 2025

**Abstract**

Where railway tracks pass through tunnels, the temperature conditions on the railway superstructure are different from those on the connecting track sections. Due to the temperature difference at the tunnel, dilatation movements occur even in cases of construction of continuously welded rail (CWR) tracks. The aim of this research is to determine the magnitude of the movements resulting from heat expansion and the normal force in the rail in the region of the tunnel gates, both in the tunnel and in the sections of track on the connecting earthworks. Ballasted and straight tracks with rail section of 54E1 are assumed in this paper.

**Keywords**

railway track, CWR track, track-tunnel interaction, change of temperature, thermal force, thermal expansion

## 1 Introduction

### 1.1 Temperature conditions in Hungary

According to the instructions of MÁV Zrt D.12.H of Hungarian Railways, that is instructions of construction and maintenance of CWR tracks, the nominal value of the neutral temperature of the rail is 23 °C and the neutral temperature zone is $23^{+5}_{-8}$ °C. The rail temperature on normal tracks can reach up to 60 °C in summer due to direct sunlight and −30 °C is recommended as the minimum value in winter, however, considering the winter weather conditions of the past 50 years, the probability of a rail temperature of −30 °C is extremely low [1].

### 1.2 Longitudinal ballast resistance based on Hungarian literature

According to Hungarian technical literatures, the longitudinal ballast resistance per unit length of track for compacted new track can be assumed to be $p$ = 5 N/mm, that for consolidated under traffic has a value within the range of 8–10 N/mm, whereas in frozen ballast the longitudinal resistance can increase up to $p$ = 10–20 N/mm. Most of the Hungarian literature communicate these values [2].

Nemesdy details accurate and approximative calculation procedures of dilatation of CWR tracks based on simplified and accurate modelling of ballast longitudinal resistance. Fig. 1(a) shows a possible diagram of tested longitudinal ballast resistance in function of displacement. Figs. 1(b) and 1(c) indicate two different bilinear approximation of the ballast resistance, in this research the one indicated in Fig. 1(c) is applied in the FEM computations. In simple calculations, the ballast resistance can be assumed to be a constant, that is shown in Fig. 1(d) [3].

### 1.3 Variation of longitudinal rail restraint and ballast resistance according to standards

The standard EN 1991-2:2003 contains recommendations of the stiffness and resistance of the rail fastenings and the ballast of the loaded and unloaded tracks, according to these the longitudinal rail restraint of the loaded rail fastening is twice higher than that of the unloaded rail fastening (Fig. 2). The standard does not specify any values, such values depend on the fastening system [4].

Key:

1. Longitudinal shear force in the track per unit length,
2. Displacement of the rail relative to the top of the supporting deck,
3. Resistance of the rail in sleeper (loaded track),
4. Resistance of sleeper in ballast (loaded track),
5. Resistance of the rail in sleeper (unloaded track),
6. Resistance of sleeper in ballast (unloaded track).

**Cite this article as:** Liegner, N. "Determination of Rail Dilatation Movements at Tunnel Gates for Ballasted Railway Tracks", Periodica Polytechnica Civil Engineering, 69(2), pp. 644–663, 2025. https://doi.org/10.3311/PPci.37989

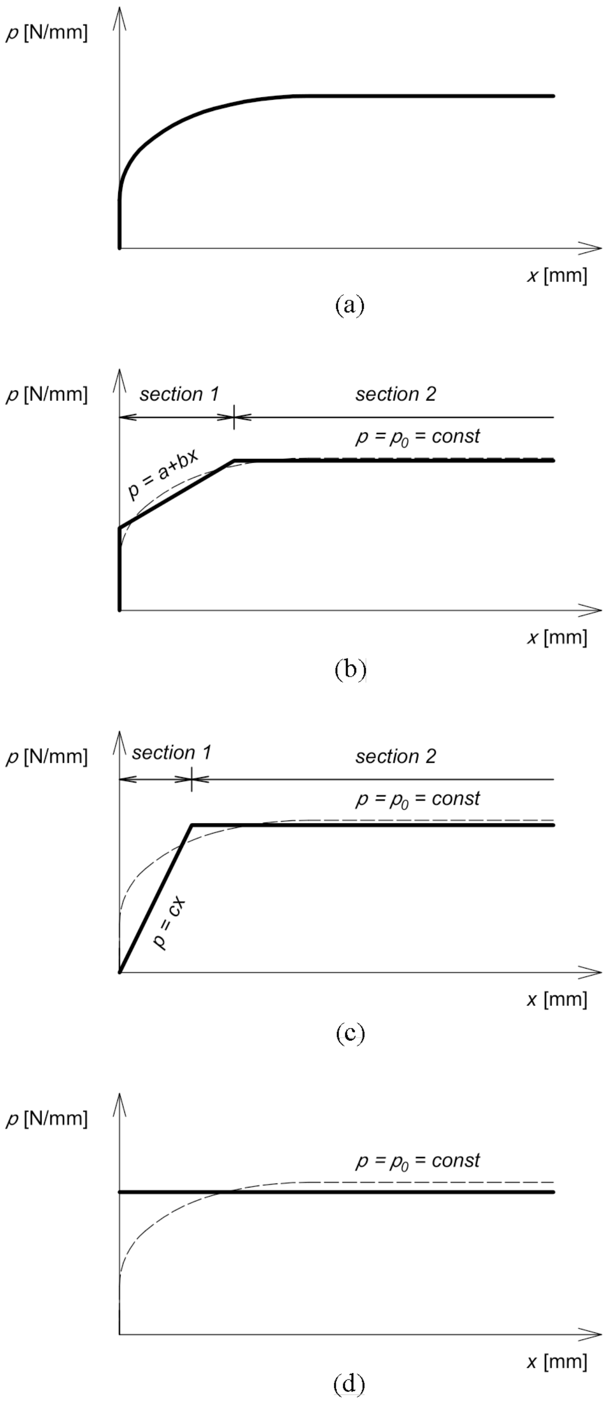


**Fig. 1** Mathematical modelling possibilities of ballast resistance according to Nemesdy [3], (a) a possible test result, (b) bilinear approximation (I), (c) bilinear approximation (II), (d) approximation by a constant

According to Track Installations [5], the resistance of the rail in the sleeper (3.) and the sleeper in the ballast (4.) is suggested to be taken for 60 kN/m in the loaded track. The resistance of the rail in the sleeper is 30 kN/m and that of the sleeper in the ballast is assumed to be 20 kN/m in the unloaded track [5].

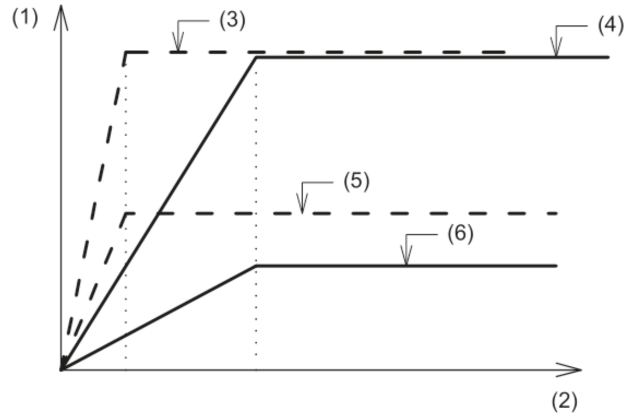


**Fig 2** Variation of longitudinal rail restraint and ballast resistance on the loaded and unloaded track according to standard EN 1991-2:2003 [4]

UIC Code 774-3 Track/bridge Interaction provides recommendations on calculations of track – bridge interaction and contains theoretical considerations that are also helpful or applicable in modelling of other track – structure interactions. It recommends that the resistance of the sleeper in ballast with moderate maintenance is 12 kN/m, in ballast with good maintenance it is 20 kN/m for unloaded tracks, and it is 60 kN/m for loaded track or in frozen ballast [6].

**1.4 Axial rail model [7]**

Free expansion or contraction of the rail due to temperature differences does not occur. A longitudinal resistance force distribution emanating from the rail fixation limits the rail displacements but may cause high forces. In Fig. 3 a small rail element is given which is subjected to a temperature increase $\Delta T$ with respect to the neutral or initial temperature, as well as a shear force $\tau(e)dx$ which opposes the displacement $e(x)$. The longitudinal force in the rail is $N(x)$. Equilibrium demands:

$$dN = \tau(x)\,dx \tag{1}$$

The total strain is the sum of temperature strain and strain according to Hooke's law:

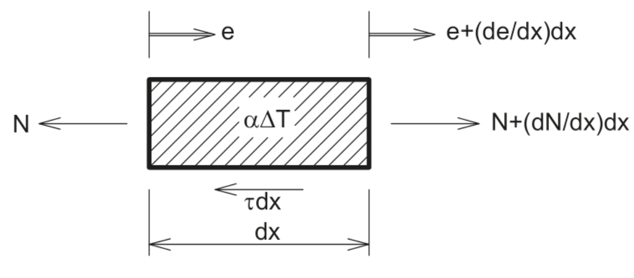


**Fig. 3** Differential rail element meant to study the temperature effect

$$\frac{de}{dx} = \alpha \Delta T + \frac{N}{EA} \tag{2}$$

In general, $\tau$ is a function of $e$, which in turn, is a function of $x$. Using the formulae (1) and (2), the following differential equation can be derived:

$$\frac{d^2e}{dx^2} - \frac{\tau(e)}{EA} = 0 \tag{3}$$

Once the displacement function $e(x)$ is found, the normal force follows from Eq. (2):

$$N = EA\left(\frac{de}{dx} - \alpha \Delta T\right) \tag{4}$$

**1.5 General international literature overview**

Mirkovic et al. have carried out a research and published the paper with the title "Determination of temperature stresses in CWR based on measured rail surface temperatures" [8] and also investigate the temperature distribution within the cross-section of the area of the rail. They also discuss the longitudinal distribution of the rail temperature along the railway line influenced by nature, clouds, trees, hills etc. They cite that in the research conducted by Chapman et al. [9] rail surface temperatures were measured using thermal camera mounted on the railway vehicle (personnel carrier) on the test section from Ruddington to Loughborough in UK. This was the first serious research where the in-situ measurements showed that rail surface temperatures were variable along the track due to the microclimate influences, such as shades of trees and buildings, cuttings, embankments, bridges, and tunnels. In addition, the study conducted in laboratory conditions by Ryan [10], showed that the maximum variation of rail surface temperature in the rail cross-section could be greater than 6 °C and that it depends on the angle at which the rail is heated. Consequently, determination of temperature stresses due to the uneven temperature distribution in continuously welded rail (CWR) in a real environment is of great importance for railway transport safety.

Popovic et al. in paper "Temperature Stresses in CWR – Experience of Serbian Railways" [11] present calculation of the temperature stresses in continuously welded rails that has great significance for the planning of maintenance activities in order to maintain traffic safety (risk of derailment due to either rail break, or track buckling). This paper presents the finite element model for calculation of rail stresses and displacements due to the temperature changes, which was developed by the authors.

Kupfer performed a PhD dissertation at the Technical University of Munich in topic of "Effects of accelerating and braking forces on longitudinal movements of the track structure" [12]. He presents laboratory test results of longitudinal rail restraint tests on rail fastenings without vertical loads and with vertical loads acting on the railhead, furthermore draws conclusions on regression curves.

Liu et al. [13] deal with the numerical simulation of temperature effects on mechanical behaviour of the railway tunnel in Tibet. They present the mechanical behaviour of tunnel lining under high geothermal temperature, which is studied by thermo-mechanical numerical method. The length of tunnel is 16 447 m, with the maximum depth 1347 m and the highest geothermal of the surrounding rock is 88 °C. Peltier et al. [14] performed numerical investigation of the convection heat transfer driven by airflows in underground tunnels. The purpose of the work is to expand on the knowledge of non-isothermal problems of internal flow common to applications conventional tunnels. Fazilova et al. [15] simulate the heat conduction processes and their impact on the stress-strain state of the continuously welded rail structure and take into account the thermal stress occurring in continuously welded rails due to deformations on the solid subgrade.

Davies et al. carried out research and published a paper [16] that concerns the recovery and use of secondary/waste heat and identifies secondary heat sources in London. London Underground (LU) railway tunnels generate significant quantities of low grade heat. There is also a requirement for active cooling to reverse the long term trend of rising tunnel temperatures. This heat is mainly generated by the braking systems of trains, although with significant contributions from aerodynamic friction and the electric motors driving the trains.

Mountain tunnels can be a direct and indirect source of geothermal energy. Tinti et al. [17] present a paper with an overview of the practice of energy lining, suggesting a procedure for the estimation of underground temperatures in mountain environments affected by the presence of a tunnel. Tunnels are sometimes severely impacted to groundwater and surface waters that also influence temperature conditions inside the tunnel [18]. Sanchis et al. [19] investigate the risk of increasing temperature, high temperatures variations, including heat wave events, due to climate change on operation of the Spanish rail network. Changing climatic conditions pose a risk to existing transport infrastructures, which are generally built based on historical climate variations. Mulholland et al. [20] assess the increased risk of extreme heat to European roads and railways with global warming.

In order to build up a model for track – tunnel interaction, it is imperative to analyse the longitudinal track resistances.

Zakeri et al. [21] present a new test method and a measurement technique was proposed to evaluate the track longitudinal resistance (TLR). The track longitudinal stiffness (TLS) and track longitudinal resistance force (TLRF) were defined based on the analyses of force-displacement curves in each test. The effect of ballast geometry on these two parameters was evaluated. De Iorio et al. [22] investigate the ballast – sleeper interaction in the longitudinal and lateral direction.

In order to support the refinement of analytical models that leverage longitudinal track resistance and stiffness, track panel pull tests (TPPTs) were executed in the laboratory [23] to expand on the values within the available literature. Further, these novel tests quantified the effect of the fastening system, crib ballast height, shoulder width, and ballast condition on the panel's longitudinal resistance and stiffness.

To improve the management of CWR rail stresses, Dersch et al [24] document the results from a field experimentation program of controlled single rail breaks (SRBs) tests that were conducted at multiple field site locations to quantify the longitudinal resistance on both timber and concrete sleeper track.

Longitudinal track resistance is one of the most critical parameters required to accurately analyze longitudinal load propagation and refine rail neutral temperature (i.e., stress-free temperature) maintenance practices. Potvin et al. [25] document common definitions of longitudinal track resistance and the two methods regularly used for its quantification: track panel pull test (TPPT) and single rail break (SRB).

In the paper of Nobakht et al. [26], the effect of vertical load on the longitudinal resistance of the ballasted railway track is investigated experimentally and numerically. First, the longitudinal resistance of a 3-m test panel with five B70 concrete sleepers under 0, 100, 200, and 300 kN vertical load were investigated, then a three-dimensional model of the track was developed using Abaqus software.

In the paper of Safizadeh et al. [27], the track longitudinal resistance (TLR) and track longitudinal stiffness (TLS) have been investigated to determine the contribution of the fastening system and sleeper in TLR and TLS through laboratory tests and a numerical model.

Alizadeh et al. [28] experimentally investigated ballasted railway tracks' longitudinal resistance and stiffness with standard and advanced Y-shaped steel sleepers. They examined the shares of various track components in providing longitudinal resistance by measuring the displacement of the track panel. Moreover, they validated the results via modelling in finite element software. In the paper of Mohammadzadeh et al. [29], the results of a field study on a test track are presented to investigate the lateral and longitudinal resistance of the ballasted track.

In order to maintain high quality performance of track transitions, track monitoring becomes even more important.

In the paper by Sun et al. [30], distributed fiber optic sensing (DFOS) was used to monitor indicators of track buckling, i.e., the axial strain, curvature, and lateral deflection along a 20-m section of curved track during the summer when ambient temperatures are highest. The DFOS provided temperature measurements along the rail; however, local variations in temperature over the cross-section were not captured by the single temperature fiber installed. According to Hong et al., the rail surface temperature can vary by up to 7 °C within the rail cross-section. Multiple temperature fibers are required to correct each strain measurement for temperature to accurately capture the track behaviour.

Liu et al. [31] present a new method for measuring longitudinal rail stress using bi-directional resistance strain gauges and develop a monitoring device for rail stress to realize long-term and multi-point measurement. They also emphasize that in CWR, the longitudinal rail stress is caused by rail temperature change and moreover, rail creep, non-uniform distribution of rail resistance, and bridge expansion/contraction lead to an additional longitudinal force in the rail through the Poisson effect, and the corresponding transverse, vertical stresses and strains are generated.

Ahmad et al. [32] introduced a new creep measurement technique using internal rail stress. They quantify the changes in rail neutral temperature due to the variation of actual rail temperature and the occurrence of rail creep in straight and curved track. Field trials showed that SFT can vary by 2–3 °C during the day. Based on this finding and the derivation of an equation for change of SFT, an improvement in utilising rail creep measurements for assessing track condition has resulted. This finding suggests that it is possible to determine the SFT throughout a day rather than just a single SFT value.

Skarova et al. [33] presented a paper that reviews and discusses the factors affecting stress-free temperature and its potential for variation along the track and over time in ballasted railway track with continuous welded rails (CWR). These include differential rail temperature changes, acceleration and braking forces, and differential track support stiffness, which in combination with a variation in the degree of longitudinal restraint offered by the rail fasteners, can result in the redistribution of stress free temperature along the track with trafficking or temperature cycling. A simple analysis of the effect of the strain associated with the development of permanent track settlements, which will change the stress-free temperature even if the longitudinal restraint to the rail is uniform, is also presented.

In this paper, a constant neutral temperature is assumed.

For a proper modelling of longitudinal rail dilatation movements, the vertical track stiffnesses, their variation and stiffness irregularities must also be analysed.

Can Shi et al. [34] provide a summary and comments in the field of tracks stiffness irregularities (TSI) and future trends from a critical point of view. Novel concepts of the critical values of TSI's and the integrated management of the track geometry and stiffness irregularities are proposed. Javaid and Choi [35] investigate the effect of track irregularities and speed on the prediction of two-way tracks' response. They developed a three-dimensional dynamic finite element (FE) model that uses tensionless stiffness between the wheel and rail to couple them. The paper of Tong et al. [36] comprehensively reviews the vertical stiffness measurement methods, values, and effective ballasted track parameters and their contribution to railway track condition monitoring.

Longitudinal forces result also in lateral displacements and in severe cases buckling. Longitudinal and lateral displacements may not be separated from each other completely, longitudinal forces may generate lateral misalignments as well.

Musazay et al. [37] study the development of lateral thermal expansion forces on a curved railway track. Three analytical methods are used to include: 1) Timoshenko thermoelastic stress analysis in cylindrical coordinate system, 2) mechanics of thin wall cylinders and 3) adaptation of a variational calculus formulation method. A fourth analysis approach is also introduced using a commercially available finite element analysis package.

The paper [38] investigates the status of lateral stability of a ballasted curved track, which is carried out under four loading scenarios in terms of the factor of safety against displacement as the indicator. The work has the potential to estimate the critical temperature differential for buckling of a curved track. In the study of Jing et al. [39], a series of single-tie push tests were performed on biblock and monoblock sleepers on a test track, where the variation of shoulder height and shoulder width has been considered as effective parameters for lateral resistance changes. Esmaeili et al. [40] present research that was allocated to investigating the effect of geogrid on the lateral resistances of both single tie and track panel via laboratory and field tests.

Tunnel construction issues are discussed by Fu [41]. Ziqiang Li et al. [42] analyse the load bearing capability and the stress distribution patterns in cases of ballastless slab tracks and ballasted tracks so the results can provide a theoretical basis for the stress analysis and design parameters of heavy-haul railway tunnel track beds.

Longitudinal extra forces, stresses and movements are generated also by rail welding that affect dilation movements. Fischer et al. [43] investigate the heat-affected zone of several rail joints executed by thermite rail welding.

A wide variety of publications are available on track – bridge interaction. Although the major topic of the publication is track – tunnel interaction, papers in track-bridge interaction may provide fruitful concepts [44–45].

Although numerous publications are available on track-structure interaction, the fluctuation of temperature on the railway track, especially at the interaction of tracks and tunnels is still open to a wide range of research into infinite depth.

In this research a constant temperature distribution is assumed for the cross-section of the rail.

## 2 Laboratory and field tests

### 2.1 Longitudinal rail restraint test of the W14 rail fastening

The longitudinal rail restraint of the rail fastening W14 was determined in the Track Laboratory of the Department of Highway and Railway Engineering, Budapest University of Technology and Economics according to standard EN 13146-1:2019 [46], under the direction of Dr. Nándor Liegner, the author of this paper. A rail section of 60E2 and the W14 fastening was assembled on a concrete sleeper and clamped firmly to a horizontal base. An increasing tensile load at a rate of 6 kN/min was applied longitudinally to the rail foot. The load and the longitudinal displacement of the rail relative to the block were measured. When the rail slipped in the fastening assembly, the load was reduced to zero rapidly and the rail displacement was measured for further two minutes. Without removing or adjusting the fastening assembly, the loading cycle was repeated further three times, with three-minute-intervals in the unloaded condition between each cycle. The average longitudinal rail resistance was calculated from the 2$^{nd}$ 3$^{rd}$ and 4$^{th}$ loading cycles, according to the calculation procedure described in the standard. The result of the first cycle was discarded. The test is shown in Fig. 4. The result of 11.06 kN has been received for the longitudinal rail restraint test of the fastening.

For the tests a data acquisition unit of Hottinger-Baldwin Messtechnik (HBM) Quantum MX840 was used with Catman Easy the software. The displacement was measured with a displacement transducer of WA20MM and a loadcell of C9B with a measuring range of 50 kN was applied both sensors of HBM.

Publications have been made by the author and a co-author on longitudinal rail restraint tests carried out on Vossloh Skl12 fastening system in the Track Laboratory of the Department of Highway and Railway Engineering, Budapest University of Technology and Economics. [47]

### 2.2 Lateral ballast resistance of track panel constructed with LM type of sleepers

The lateral ballast resistance of a track panel with LM type of concrete sleepers was determined by the Track Laboratory of the Department of Highway and Railway Engineering, Budapest University of Technology and Economics under the direction of Dr. Nándor Liegner. A track panel consisting of four LM types of concrete sleepers, W14 rail fastenings and two rails was constructed in a ballast bed. The shoulder of the ballast had a width of 0.45 m. The ballast was compacted by manual machines but was not stabilized. The track panel was loaded laterally three times by hydraulic actuators, the load and the displacement of the sleepers were measured. The lateral ballast resistance per unit length of track has been resulted to be 7.54 N/mm belonging to the highest load, and it is 7.39 N/mm at the load inducing 2 mm's of lateral displacement of the track panel.

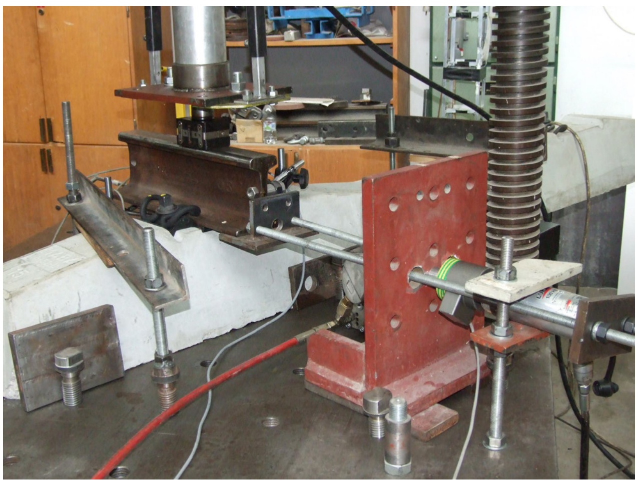

**Fig. 4** Arrangement of the longitudinal rail restraint test

### 2.3 Longitudinal ballast resistance of track panel constructed with LM type of sleepers

The longitudinal ballast resistance of track panel constructed of LM type of concrete sleepers was determined by the Track Laboratory of the Department of Highway and Railway Engineering, Budapest University of Technology and Economics under the direction of Dr. Nándor Liegner. A track panel consisting of four LM types of concrete sleepers, K (Geo) rail fastenings and two rails was constructed in a ballast bed, that had a shoulder width of 0.40 m. The ballast was compacted by petrol engine vibrators. The track panel was pushed by two hydraulic actuators, the load was measured by two load cells of HBM C9B 50 kN, and the displacement was measured by two inductive displacement transducers of type HBM WA20MM. The longitudinal ballast resistance has been obtained to be between 5.3 and 5.9 kN in compacted but not consolidated ballast bed.

## 3 General structure of the computation model

### 3.1 Basic concepts

For this research I built a finite element model using AxisVM X5 software. The models are for half cross section of the superstructure. The railway track was modelled with a two-dimensional beam model with line-supported Euler-Bernoulli elements, with the same characteristics as the 54E1 system rail [48, 49]:

- area of cross-section: 6977 $mm^2$
- modulus of elasticity: 215 000 $N/mm^2$
- modulus of linear heat expansion: $1.15 \cdot 10^{-5}$ 1/°C.

Continuously welded rails are assumed and there are no rail expansion devices at the tunnel gates.

Only straight tracks are examined in this paper where the lateral stability is considered to be a pre-condition. In curved tracks, lateral stability may arise an additional problem, however it is a topic of a different paper.

### 3.2 Supports, properties of the ballast

A properly maintained, consolidated ballast can have a longitudinal resistance of 8 to 10 N/mm per rail, compared to 5 N/mm for newly laid ballast. Accordingly, the limiting longitudinal resistance of the ballast was assumed to be 5 N/mm for modelling the newly constructed track. Due to the vertical loads from the self-weight of the vehicles, the longitudinal resistance of the track increases and it can be assumed to be twice or three times higher, that is 10 to 15 N/mm. In this research a sensitivity analysis has been carried out and three models have been built up:

- the longitudinal ballast resistance is 7 N/mm, that is less than the braking load,
- the longitudinal ballast resistance is 10 N/mm, that is equal to the braking load,
- the longitudinal ballast resistance is 15 N/mm, that is more than the braking load.

For the support a bilinear elastic and plastic stiffness has been assumed as shown in Fig. 1(c). Within the elastic part, the longitudinal stiffness has been assumed on the basis that the maximum longitudinal load per rail is 4.8 kN, the elastic displacement of the ballast is 1 mm, the sleeper spacing is 0.6 m and it will result in 4.8 (kN) / 1 mm / 0.6 m = 8 kN/mm/m in the unloaded models. In case of the loaded models the longitudinal elasticity has been taken to

- 8 / 5 × 7 = 11.2 kN/mm/m in case of a ballast resistance of 7 N/mm,
- 8 / 5 × 10 = 16.0 kN/mm/m in case of a ballast resistance of 10 N/mm,
- 8 / 5 × 15 = 24.0 kN/mm/m in case of a ballast resistance of 15 N/mm.

Of course, a sensitivity analysis could be carried out to analyse how longitudinal rail displacements will vary by changing the elasticity of the ballast, but due to limit of the extent of this paper, such analysis will fall into another research paper. These values have been chosen based on our field measurements with LM sleepers, but different sleeper types may result in different elasticity and limit values.

### 3.3 Loads

Dilatation movements and longitudinal internal forces in a railway superstructure result from two main effects:

- change of temperature in the rail,
- braking and acceleration of the trains.

#### 3.3.1 Change of temperature in the rail

As it was already mentioned in Section 1.1, according to the instructions of MÁV Zrt D.12.H of Hungarian Railways, the nominal value of the neutral temperature of the rail is 23 °C and the neutral temperature zone is $23^{+5}_{-8}$ °C. The rail temperature on normal tracks can reach up to 60 °C in summer due to direct sunlight and −30 °C is recommended as the minimum value in winter [48].

In tunnels, the lack of sunlight and the internal heat of the ground create significantly different temperature conditions. The resulting temperature conditions depend to a great extent on the length of the tunnel, with a short tunnel having only a small difference in air temperature compared to the air outside the tunnel, while long tunnels have similar temperatures in winters and summers. To model this, a sensitivity analysis has been carried out, where several models have been built, two examples are the following:

- Case 'A' represents a medium long tunnel and
- Case 'B' models a long tunnel in respect of temperature conditions.

In case A, the highest rail temperature in the tunnel is taken as +30 °C in summer and the lowest rail temperature is taken as −5 °C in winter. The winter temperature change in the tunnel is +28 − (−5) = 33 °C, and outside +28 − (−30) = 58 °C. The summer temperature change is +60 − 15 = 45 °C for the track section on the earthworks and +30 − 15 = 15 °C in the tunnel [49].

In case "B", the highest rail temperature in the tunnel was taken as +20 °C in summer and the lowest rail temperature as +15 °C in winter. The winter temperature change in the tunnel +28 − (+15) = 13 °C and outside the tunnel +28 − (30) = 58 °C. The summer temperature change is +60 − 15 = 45 °C for the track section on the earthworks and +20 − 15 = 5 °C in the tunnel.

In the calculations, sudden change of temperature is modelled. At the tunnel entrance, we assume that, for example, in winter, one rail cross-section has a temperature of −30 °C and the one immediately adjacent to it has +15 °C. In reality, the temperature change is distributed over a given length, depending on several factors. A sensitivity analysis can be performed and the results can be used to comment on how the length of the temperature change affects the results. This is the subject of future research and a future publication.

The temperature variations are assumed to occur annually, however with this model temperature changes occurring in any time intervals, such as day-night, or monthly, etc. can be simulated and calculated. Day-night temperature changes normally do not raise a problem in operation in Hungary. Long-term creeps are not possible to be modelled with this software.

In this research a constant temperature is assumed for each point of a cross-section of the rail. In this paper the results obtained in Case 'A' are presented.

#### 3.3.2 Braking and acceleration forces

According to the standard EN 1991-2 Eurocode-1, the distributed load that can be taken into account on the loaded section of the braking is 20 kN/m with a maximum value of 6000 kN that will result in total length of 300 m. The effect of acceleration is considered with a uniformly distributed load of 33 kN/m/track, with a maximum value of 1000 kN. Of braking and acceleration, it is the braking that is significant [48, 49].

Regarding the braking force, it should be noted that a distributed braking force of 20 kN/m/track can only be produced by a locomotive with rail brakes. Freight trains equipped with conventional air brakes can exert a braking force of only 15 kN/m/track for a wagon with a self-weight of $G = 900$ kN, $\mu = 0.25$ coefficient of adhesion friction and $l = 15.00$ m length, where $\mu = 0.25$ is considered high. Although high-speed passenger vehicles (e.g. RailJet trains) are equipped with high-power rail brakes, their relatively lightweight construction and long length mean that they can only apply a maximum distributed braking force of 50 000 (kg) × 3 (m/s$^2$) / 26.40 (m) = 5.68 kN/m/track [49].

### 3.3.3 Combination of loads

The load combinations consist of the thermal load in winter and summer and the braking load over a length of 300 m. In order to determine the load positions generating the standard, significant forces, the distributed load modelling braking to the right was shifted in steps of 50 m from its position shown in Fig. 5(a) to the load position shown in Fig. 5(b). The load positions for braking left were mirror images of braking right. All load positions were combined with both winter and summer thermal loads [49].

The temperature change (also) occurs on the unloaded track, while the acceleration-braking force can only occur on the track loaded by the weight of the trains. For the loading cases where the displacements and normal forces due to only temperature changes were considered, the longitudinal ballast resistance of the unloaded track of $p = 5$ N/mm was taken into account. When the displacements and normal forces due to braking were determined, increased longitudinal ballast resistances listed in Section 3.1 were assumed for the section of the track where the braking force acts. For these cases, of course, different models had to be built up.

## 4 Results of internal forces and displacements from the effects of temperature change, with the assumption of a ballast resistance of p = 5 N/mm

The normal force in the rail due to temperature changes and the heat expansion of the rail can be considered as a slow process in time in a mechanical sense, which occurs on a track without the load of trains. The displacements and normal forces calculated from the temperature change in the unloaded model at the tunnel entrance are shown in Table 1. The displacement of the rail at summer temperature is shown in Fig. 6. The normal force in the rail at summer temperatures is illustrated in Fig. 7.

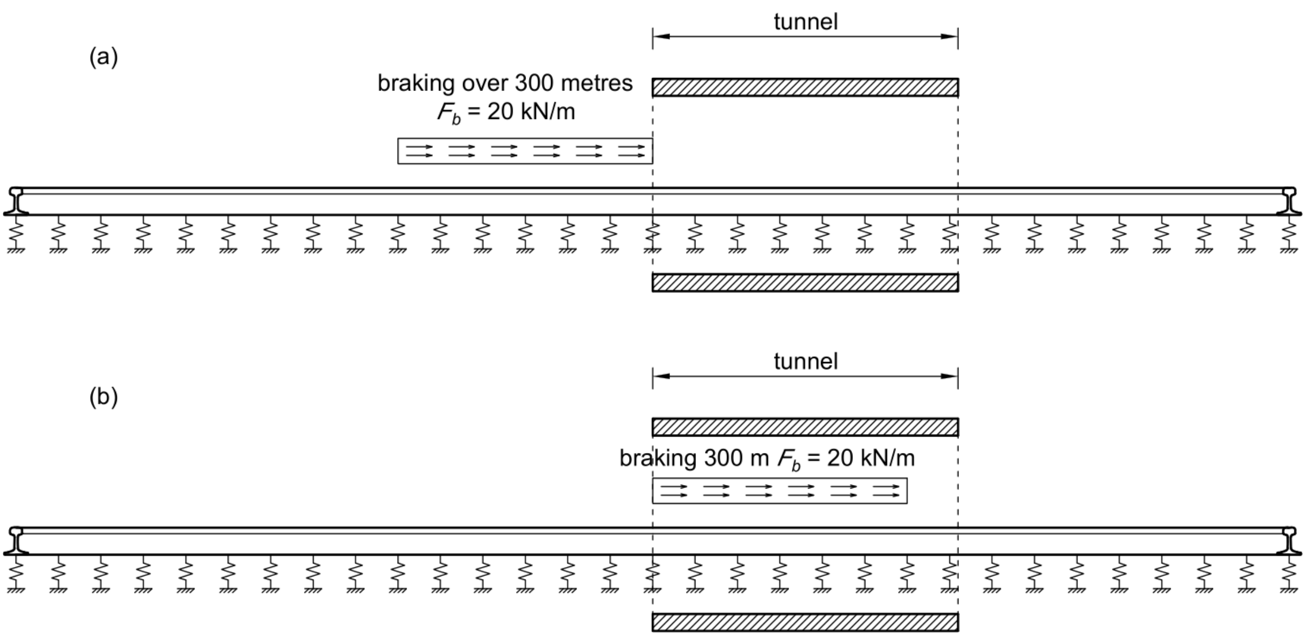


**Fig 5** Modelling the effect of braking, (a) starting position of braking, (b) end position of braking

**Table 1** Effects in the unloaded rail from the change of temperature

| Load case | Change of temperature | Track section | Longitudinal displacement of rail, $e_x$ [mm] | Normal force in the rail, $N$ [kN] |
|---|---|---|---|---|
| | | track on earthwork | 0 | 1001.67 |
| | | gate of tunnel | −3.416 | 785.79 |
| 1 | Winter | extreme value | −3.416 | 1001.67 |
| | | location of extreme value | at the gate | track on earthwork |
| | | tunnel | 0 | 571.81 |
| | | track on earthwork | 0 | −777.15 |
| | | gate of tunnel | 4.781 | −518.10 |
| 2 | Summer | extreme value | 4.781 | −777.78 |
| | | location of extreme value | at the gate | track on earthwork |
| | | tunnel | 0 | −259.93 |

Under the temperature change and bedding conditions assumed in the unloaded model [49]:

- the normal force in the rail at winter temperature is 571.81 kN in the tunnel and 1001.67 kN outside the tunnel,
- the maximum longitudinal rail displacement at winter temperatures is 3.42 mm, which is generated at the tunnel entrance,
- the normal force in the rail at summer temperature is 259.93 kN in the tunnel and 777.15 kN outside the tunnel,
- the maximum longitudinal rail displacement at summer temperatures is 4.78 mm, which occurs at the tunnel entrance.

The gates of the tunnel that are beginnings and ends of the tunnel are indicated by a GT sign.

## 5 Results of internal forces and displacements with the assumption of a ballast resistance of *p* = 7 N/mm over the braking section

Under the load of trains, the longitudinal resistance of the ballast bed increases significantly. On the actual track, the longitudinal elasticity and the longitudinal resistance of the ballast depend on the magnitude of the vertical load. Movements of heat expansion occur in the unloaded ballast with lower resistance and are then compounded by displacements and internal forces in the bedding with increased stiffness and resistance due to the vertical loads of the trains.

However, the specificity of the model is that only one elasticity data can be given at a stage. For this reason, a constant longitudinal ballast resistance — limiting force — of $p = 7$ N/mm is considered for the 300 m long section of track on which the braking force is applied, while $p = 5$ N/mm is considered for other sections. The drawback, however, is that

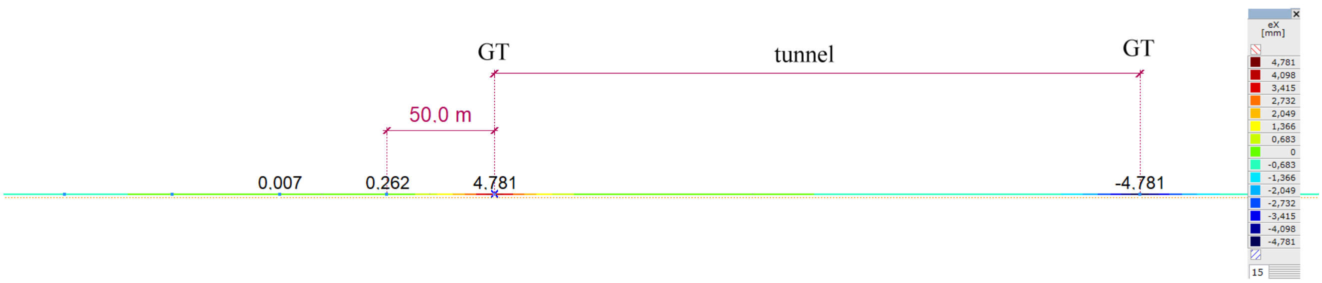


**Fig. 6** Longitudinal displacement [mm] of the unloaded rail due to summer change of temperature

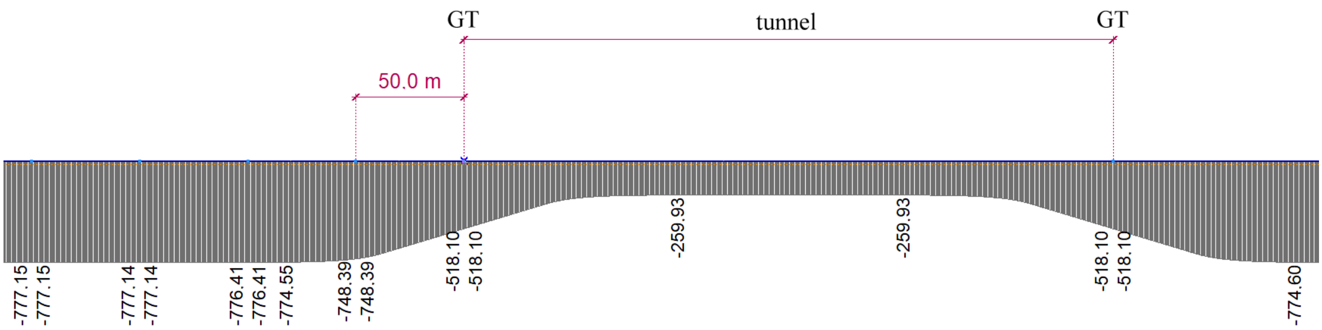


**Fig. 7** Normal forces [kN] in the unloaded rail due to summer change of temperature

the displacements and stresses due to temperature changes are also calculated assuming a resistance of $p = 7$ N/mm for the 300 m long section loaded with the braking force.

### 5.1 Effects of temperature changes without braking force

The longitudinal displacements and the normal forces in the rails resulting from each load case and load combination in the loaded model are summarized in Table 2. If the above model is subjected only to thermal loads — load cases 1 and 2 as shown in Table 2 — the maximum rail displacement is obtained at load positions I and VII, its value is 2.917 mm in winter and 4.063 mm in summer. The maximum rail displacements due to change of temperature without braking is generated at the gate of the tunnel.

### 5.2 Effects of braking alone

The distributed load of braking on one rail is 10 kN/m. The longitudinal elasticity of the ballast is assumed to be $K = 11.2$ kN/mm/m, the limiting force is chosen to be $p = 7$ N/mm that is less than the braking force. The possibility of this case is rare in reality, although the results simulate a case what could happen if the braking force is greater than the ballast resistance. In this case the load over 1 m length is greater than what the support can react, therefore the reaction forces will be distributed over longer length than that of the braking that is 300 m. As a consequence of this, a high normal force is generated in the rail, whose magnitude is ±450 kN. In front of the braking, it is compression, and it is tension behind the braking looking in the direction of the braking force. For all load cases, the maximum force in the rail is developed at the points at the beginning and end of the braking and the maximum displacement of the rail is developed in the middle of the braking section.

If only braking or acceleration is applied to the track without temperature change – load cases 3 and 4 of Table 2 –, the normal forces in the rail due to right braking starting 300 m in front of the gate of the tunnel is shown in Fig. 8. Fig. 9 indicates the longitudinal displacement of the rail due to right (→) braking starting at 300 m in front of the tunnel. The maximum longitudinal displacement of the rail is 36.271 mm whose position is at the middle point of the braking. The illustrations of "10.00" on Figs. 8 and 9 in blue indicate the braking force of 10.00 kN/m acting on one rail.

### 5.3 Effects of combination of change of temperature and braking with the assumption of a ballast resistance of p = 7 N/mm over the braking section

The normal force in the rail and the rail displacements due to the combination of change of temperature and braking are summarized in Table 2, load combinations 5–8. The maximum tensile force is generated in the rail in winter and due to a right (→) braking that starts 300 m in front of the tunnel. Its value is 1400.31 kN and its position coincides with the starting point of the braking that is 300 m before the gate of the tunnel (Fig. 10). The location of the minimum and maximum value of the normal force in the rail coincides with the starting and end point of the braking. By evaluating the normal forces in Table 2, load combinations 5–8, the normal

**Table 2** Maximum values of the rail displacements and the normal forces in the rail resulting from load combinations, $p = 7$ N/mm on the loaded section

| | Load combination | Effect | Number of load case and position of the beginning of the braking in front of the tunnel | | | | | | |
|---|---|---|---|---|---|---|---|---|---|
| | | | I.<br>300 m | II.<br>250 m | III.<br>200 m | IV.<br>150 m | V.<br>100 m | VI.<br>50 m | VII.<br>0 m |
| 1. | winter | displacement $e_x$ [mm] | −2.917 | −2.529 | −2.529 | −2.529 | −2.529 | −2.529 | −2.917 |
| 2. | summer | displacement $e_x$ [mm] | 4.063 | 3.505 | 3.505 | 3.505 | 3.505 | 3.505 | 4.063 |
| 3. | braking → | displacement $e_x$ [mm] | 36.271 | 36.271 | 36.271 | 36.271 | 36.271 | 36.271 | 36.271 |
| | | normal force N [kN] | 450.00 | 450.00 | 450.00 | 450.00 | 450.00 | 450.00 | 450.00 |
| 4. | braking ← | displacement $e_x$ [mm] | −36.271 | −36.271 | −36.271 | −36.271 | −36.271 | −36.271 | −36.271 |
| | | normal force N [kN] | 450.00 | 450.00 | 450.00 | 450.00 | 450.00 | 450.00 | 450.00 |
| 5. | winter + brake → | displacement $e_x$ [mm] | 28.532 | 21.301 | 15.140 | 10.047 | 15.314 | 29.654 | 44.029 |
| | | normal force $N$ [kN] | 1400.31 | 1345.47 | 1290.63 | 1235.80 | 1182.04 | 1181.82 | 1181.82 |
| 6. | winter + brake ← | displacement $e_x$ [mm] | −54.326 | −62.049 | −70.176 | −73.570 | −68.924 | −57.887 | −44.029 |
| | | normal force $N$ [kN] | 1350.14 | 1312.03 | 1274.04 | 1237.40 | 1205.68 | 1185.05 | 1181.82 |
| 7. | summer + brake → | displacement $e_x$ [mm] | 59.204 | 68.627 | 78.201 | 81.520 | 76.387 | 63.686 | 47.443 |
| | | normal force $N$ [kN] | −1101.27 | −1056.90 | −1012.91 | 971.30 | 935.21 | −909.68 | −903.34 |
| 8. | summer + brake ← | displacement $e_x$ [mm] | −28.147 | −19.763 | −12.712 | −7.250 | −13.286 | −30.192 | −47.442 |
| | | normal force $N$ [kN] | −1173.07 | −1108.11 | −1041.40 | −974.79 | −909.43 | −903.34 | −903.34 |

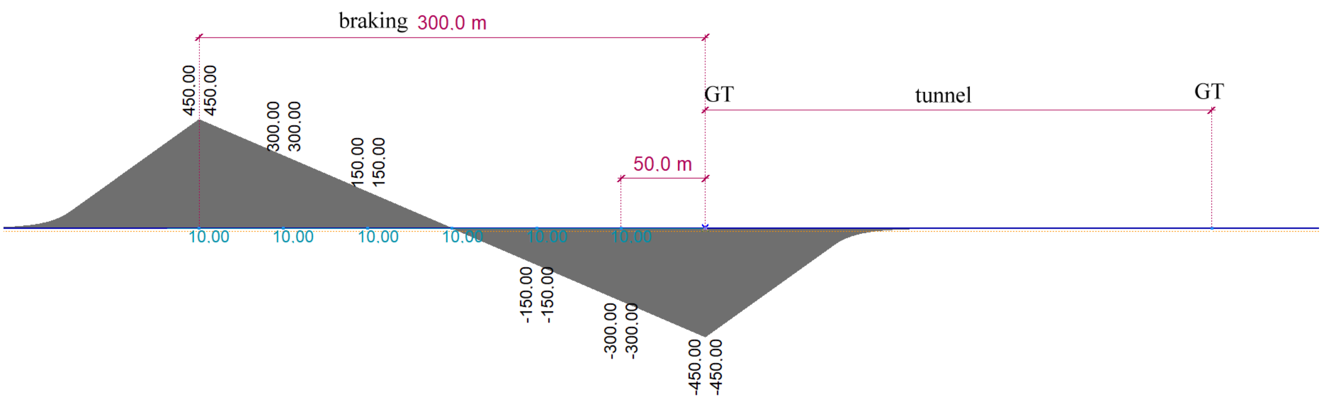


**Fig. 8** Normal forces [kN] in the rail due to right (→) braking starting 300 m in front of the gate of the tunnel, $p$ = 7 N/mm

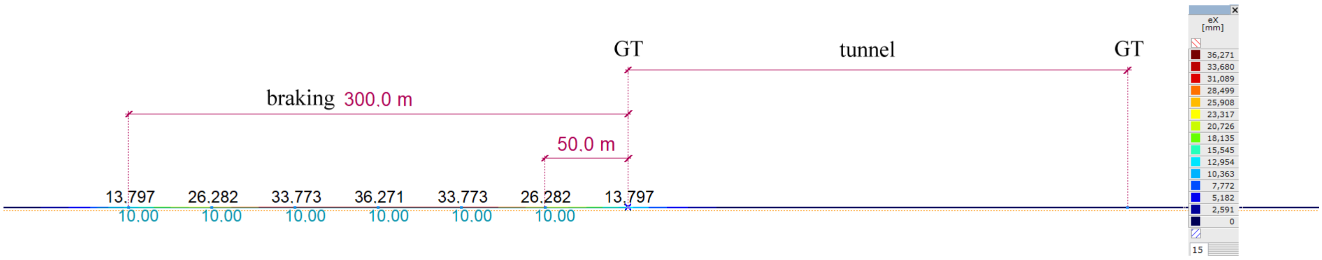


**Fig. 9** Longitudinal displacement [mm] of the rail due to right (→) braking starting at 300 m in front of the tunnel, $p$ = 7 N/mm

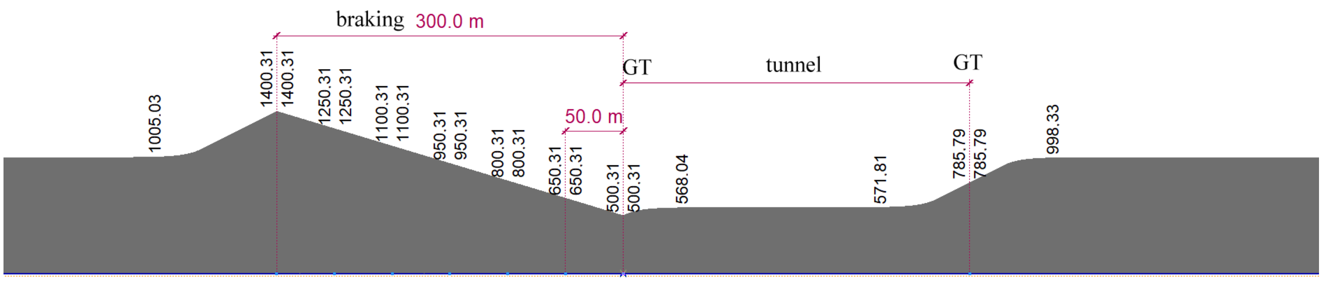


**Fig. 10** Normal forces [kN] in the rail due to winter temperature plus right (→) braking starting at 300 m in front of the tunnel, $p$ = 7 N/mm

forces in the rail are significantly higher due to the load combinations including braking than those due to only change of temperature, included in Table 1. As in Section 5.2, it can also be concluded that if the limiting force of the ballast resistance is less than the uniformly distributed braking load, the normal forces in the rail will be significantly higher due to load combinations including braking forces than those due to only change of temperature.

The maximum normal forces in the rail due to summer temperature and left (←) braking starting 300 m in front of the gate of the tunnel is indicated in Fig. 11, its value is 1173.07 kN. The shape is similar to that in winter temperature, but of winter and summer, this is the winter that is more significant.

The calculated maximum longitudinal displacement of the rail is 81.52 mm, which is obtained under summer temperature variation and rightward (→) braking starting at 150 m in front of the tunnel from the earthwork section into the tunnel (load combination 7) and its position is at the gate of the tunnel. In this load position the middle point of the braking is at the gate. The longitudinal displacement of the rail is illustrated in Fig. 12. By evaluating the longitudinal displacements of Table 2, load combinations 5–8, it can also be concluded that if the limiting force of the ballast resistance is less than the uniformly distributed braking load, significant longitudinal displacements of the rail will be resulted. The maximum displacement occurs – as we have seen it in Section 5.2 – at the middle

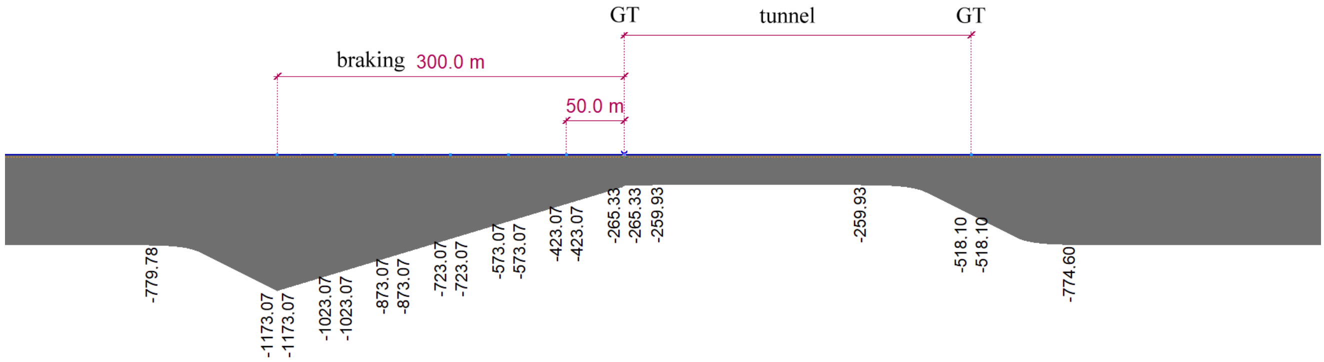


**Fig. 11** Normal force [kN] in the rail due to summer temperature plus left (⟵) braking starting at 300 m in front of the tunnel, $p$ = 7 N/mm

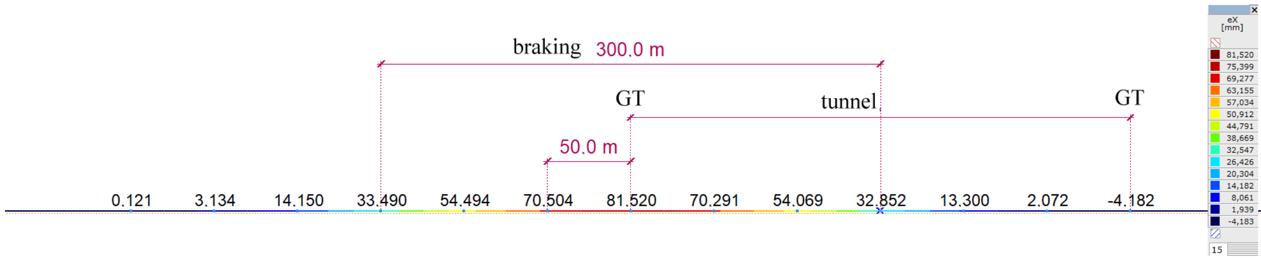


**Fig. 12** Displacement [mm] of the rail due to summer temperature plus right (⟶) braking starting at 150 m in front of the tunnel, $p$ = 7 N/mm

point of the braking. The maximum rail displacement is resulted if the middle point of the braking coincides with the point of the sudden change of temperature, that happens always at the gate of the tunnel.

The FEM software Axis does the static calculations so that it applies the loads in normally 50 increments, therefore it is not possible to separate elastic and residual displacements.

Due to winter temperature the maximum rail displacement is 73.57 mm and it occurs at the gate of the tunnel in case of left (⟵) braking that starts 150 m before the tunnel.

As it has already been mentioned in Section 5.2, the possibility of huge displacements of 70 to 80 mm is very rare in reality, although the results simulate a theoretical case what could happen if the braking force is greater than the ballast resistance. On tracks with clean ballast of good quality, well compacted and consolidated, the longitudinal ballast resistance under the load of the trains can be considered to be 30 N/mm per rail [5, 6, 11] that is higher than the braking force of 10 kN/mm. A loaded ballast resistance of less than 10 kN/mm may occur only directly after laying newly constructed ballast or ballast screening, however in such cases a speed restriction of 40 km/h or appropriate restrictions are ordered. By dynamic ballast stabilizing machines and the self-compaction of the ballast under traffic, the ballast resistance increases rapidly higher than the braking force of 10 kN/mm. Since the time duration of the ballast resistance of less than the braking force is limited to short time periods directly after construction or maintenance works, this situation does not have much significance on the life cycle of the track. This could be analysed in a different research and the results published in a separate paper.

## 6 Results of internal forces and displacements with the assumption of a ballast resistance of $p$ = 10 N/mm over the braking section

As it has already been introduced, under the load of trains, the longitudinal resistance of the ballast bed increases significantly. In this Section the longitudinal ballast resistance – limiting force – of $p$ = 10 N/mm is considered for the 300 m long section of track on which the braking force is applied, while $p$ = 5 N/mm is considered for other sections. The drawback, again, is that the displacements and stresses due to temperature changes are also calculated assuming a resistance of $p$ = 10 N/mm for the 300 m long section loaded with the braking force. The calculations presented in this Section simulate a case when the braking force is equal to the ballast resistance.

### 6.1 Effects of temperature changes without braking force

The longitudinal displacements and the normal forces in the rails resulting from each load case and load combination in the loaded model are summarized in Table 3. If the above model is subjected only to thermal loads – load cases 1 and 2 as shown in Table 3 — the maximum rail displacement is

**Table 3** Maximum values of the rail displacements and the normal forces in the rail resulting from load combinations, $p$ = 10 N/mm on the loaded section

| | Load combination | Effect | Number of load case and position of the beginning of the braking in front of the tunnel | | | | | | |
|---|---|---|---|---|---|---|---|---|---|
| | | | I.<br>300 m | II.<br>250 m | III.<br>200 m | IV.<br>150 m | V.<br>100 m | VI.<br>50 m | VII.<br>0 m |
| 1. | winter | displacement $e_x$ [mm] | −2.442 | −1.864 | −1.864 | −1.864 | −1.864 | −1.864 | −2.442 |
| 2. | summer | displacement $e_x$ [mm] | 3.379 | 2.547 | 2.547 | 2.547 | 2.547 | 2.547 | 3.379 |
| 3. | braking → | displacement $e_x$ [mm] | 0.625 | 0.625 | 0.625 | 0.625 | 0.625 | 0.625 | 0.625 |
| | | normal force $N$ [kN] | ±40.13 | ±40.13 | ±40.13 | ±40.13 | ±40.13 | ±40.13 | ±40.13 |
| 4. | braking ← | displacement $e_x$ [mm] | −0.625 | −0.625 | −0.625 | −0.625 | −0.625 | −0.625 | −0.625 |
| | | normal force $N$ [kN] | ±40.13 | ±40.13 | ±40.13 | ±40.13 | ±40.13 | ±40.13 | ±40.13 |
| 5. | winter + brake → | displacement $e_x$ [mm] | −1.488 | −0.778 | −0.776 | −0.776 | −0.776 | −0.778 | −1.460 |
| | | normal force $N$ [kN] | 1041.80 | 1041.80 | 1041.80 | 1041.80 | 1041.79 | 1040.76 | 1001.67 |
| 6. | winter + brake ← | displacement $e_x$ [mm] | −10.110 | −18.368 | −23.326 | −24.977 | −23.315 | −18.721 | −9.967 |
| | | normal force $N$ [kN] | 1001.67 | 1001.67 | 1001.67 | 1001.67 | 1001.67 | 1001.67 | 1001.67 |
| 7. | summer + brake → | displacement $e_x$ [mm] | 13.893 | 23.206 | 28.793 | 30.653 | 28.762 | 23.001 | 13.632 |
| | | normal force $N$ [kN] | −777.15 | −777.15 | −777.15 | −777.15 | −777.15 | −777.15 | −777.15 |
| 8. | summer + brake ← | displacement $e_x$ [mm] | 2.093 | 1.119 | 1.117 | 1.117 | 1.117 | 1.119 | 2.039 |
| | | normal force $N$ [kN] | −817.29 | −817.29 | −817.28 | −817.28 | −817.28 | −815.99 | −777.15 |

obtained at load positions I and VII, its value is value of 2.442 mm in winter and 3.379 mm in summer. The maximum rail displacements due to change of temperature without braking is generated at the gate of the tunnel.

### 6.2 Effects of braking alone

If only braking or acceleration is applied to the track without temperature change – load cases 3 and 4 of Table 3 – there is no significant displacement or normal force in the track. The distributed force of braking on a rail is 10 kN/m, the longitudinal elasticity of the ballast is $K$ = 16 kN/mm/m, the resistance is $p$ = 10 N/mm and the resulting longitudinal displacement is $e_x$ = 0.625 mm. At the beginning and at the end of the braking section, a normal force of 40.13 kN is generated in the rail due to the resistance of the neighboring unloaded ballast of $p$ = 5 N/mm.

Fig. 13 indicates the longitudinal displacement of the rail due to right (→) braking starting at 300 m in front of the tunnel. The normal forces in the rail due to right braking starting 300 m in front of the gate of the tunnel is shown in Fig. 14. With the comparison of Figs. 8 and 14, it can be seen that if the limiting force of the ballast resistance is equal or higher than the uniformly distributed braking load, no significant normal forces are generated in the rail. If however the ballast resistance is less than the braking force, then significant internal tensile and compression forces are generated in the rail (previous Fig. 8).

### 6.3 Effects of combination of change of temperature and braking with the assumption of a ballast resistance of $p$ = 10 N/mm over the braking section

The longitudinal displacements for the load combinations and their load positions, consisting of the winter and summer temperature variations and the braking forces to the right and left, and the normal force in the rail are summarized in Table 3, load combinations 5–8.

The maximum normal forces in the rail due to winter temperature and right braking starting 150 m in front of the gate of the tunnel is indicated in Fig. 15, p = 10 N/mm, its value is 1041.80 kN. By evaluating the normal forces in Table 3, load combinations 5–8, it can be concluded that the normal forces in the rail are not significantly higher due to the

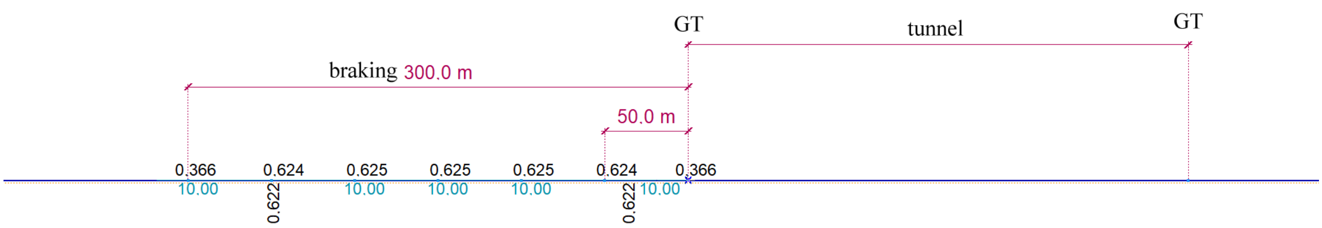


**Fig. 13** Longitudinal displacement [mm] of the rail due to right (→) braking starting at 300 m in front of the tunnel, $p$ = 10 N/mm

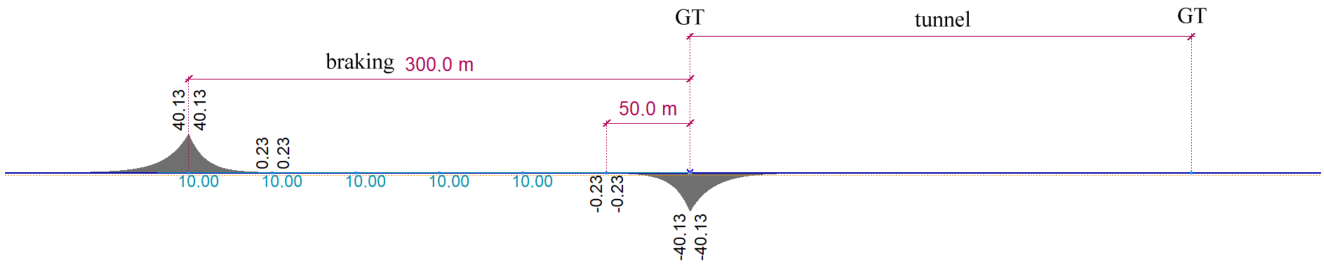


**Fig. 14** Normal forces [kN] in the rail due to right (→) braking starting 300 m in front of the gate of the tunnel, $p$ = 10 N/mm

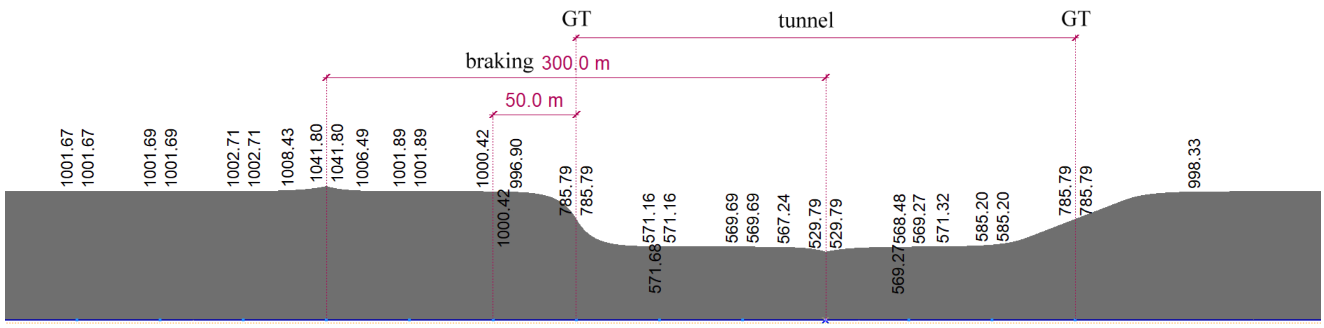


**Fig. 15** Normal forces [kN] in the rail due to winter temperature and right braking starting 150 m in front of the gate of the tunnel, $p$ = 10 N/mm

load combinations including braking than those due to only change of temperature, included in Table 1. As in Section 6.2, it can also be concluded that if the limiting force of the ballast resistance is equal or higher than the uniformly distributed braking load, the normal forces in the rail will not be significantly higher due to load combinations including braking forces than those due to only change of temperature.

The calculated maximum longitudinal displacement of the rail is 30.65 mm, which is obtained under summer temperature variation and rightward braking starting at 150 m in front of the tunnel from the earthwork section into the tunnel (load combination 7) and its position is at the gate of the tunnel. The longitudinal displacement of the rail is illustrated in Fig. 16. By comparing the longitudinal displacements of Tables 2 and 3, load combinations 5–8, it can also be concluded that if the limiting force of the ballast resistance is equal or higher than the uniformly distributed braking load, the longitudinal displacement of rail will be resulted significantly lower, than in case that the ballast resistance is less than the braking force.

The illustrations of "10.00" on Figs. 14 and 15 indicate the braking load of 10.00 kN/m acting on one rail.

## 7 Results of internal forces and displacements with the assumption of a ballast resistance of $p$ = 15 N/mm over the braking section

In this Section a longitudinal ballast resistance of $p$ = 15 N/mm has been assumed on the track sections with braking forces, that is significantly greater than the braking load, and 5 N/mm on other sections.

### 7.1 Effects of temperature changes without braking force

The longitudinal displacements and the normal forces in the rails resulting from each load case and load combination

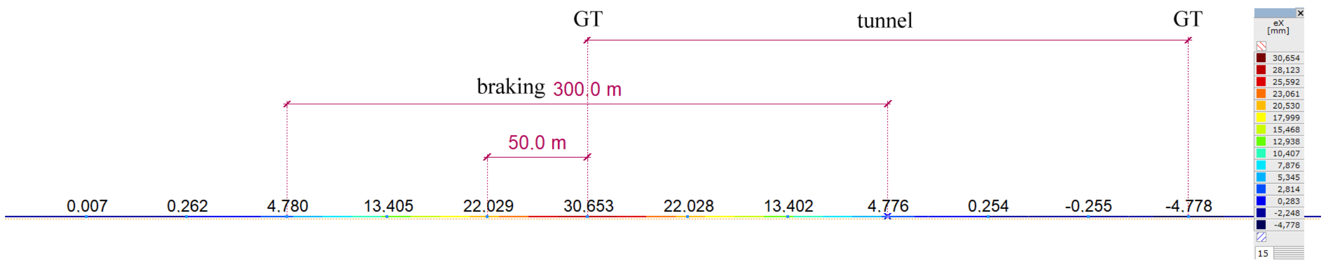


**Fig. 16** Longitudinal displacement [mm] of the rail due to summer temperature and right (→) braking starting at 150 m in front of the tunnel, $p$ = 10 N/mm

in the loaded model are summarized in Table 4. If the above model is subjected only to thermal loads – load cases 1 and 2 as shown in Table 4 – the maximum rail displacement is obtained at load positions I and VII, its value is 1.975 mm in winter and 2.707 mm in summer. The maximum rail displacements due to change of temperature without braking is generated at the gate of the tunnel.

### 7.2 Effects of braking alone

If only braking or acceleration is applied to the track without temperature change – load cases 3 and 4 of Table 4 – there is no significant displacement or normal force in the track. The distributed force of braking on a rail is 10 kN/m, the longitudinal elasticity of the ballast is $K$ = 24 kN/mm/m, the resistance is $p$ = 15 N/mm and the resulting longitudinal displacement is $e_x$ = 0.417 mm. At the beginning and at the end of the braking section, a normal force of 28.95 kN is generated in the rail due to the resistance of the neighboring unloaded ballast of $p$ = 5 N/mm.

The normal forces in the rail due to right braking starting 300 m in front of the gate of the tunnel is shown in Fig. 17. With the comparison of Figs. 8, 14 and 17, it can be seen that if the limiting force of the ballast resistance is equal or higher than the uniformly distributed braking load, no significant normal forces are generated in the rail.

### 7.3 Effects of combination of change of temperature and braking

The longitudinal displacements for the load combinations and their load positions, consisting of the winter and summer temperature variations and the braking forces to the right and left, and the normal force in the rail are summarized in Table 4, load combinations 5–8.

The maximum normal forces in the rail due to winter temperature and right braking starting 150 m in front of the gate of the tunnel is indicated in Fig. 18, its value is 1030.62 kN. By evaluating the normal forces in Table 4, load combinations 5–8, it can be concluded that the normal forces in the rail are not significantly higher due to the load combinations including braking than those due to only change of temperature, included in Table 1. As in Section 7.2, it can also be concluded that if the limiting force of the ballast resistance is equal or higher than the uniformly distributed braking load, the normal forces in the rail will not be significantly higher due to load combinations including braking forces than those due to only change of temperature.

The calculated maximum longitudinal displacement of the rail is 4.990 mm, which is obtained under summer temperature variation and rightward braking starting at 150 m in front of the tunnel from the earthwork section into the tunnel (load combination 7) and its position is at the gate of the tunnel. The longitudinal displacement of the rail is illustrated in Fig. 19. The maximum displacement of the rail is 3.624 mm due to the combined effect of winter temperature variation and braking. By comparing the longitudinal displacements of Tables 2 and 4, load combinations 5–8, it can also be concluded that if the limiting force of the ballast resistance is remarkably higher than the uniformly distributed braking load, the longitudinal displacement of rail will be only slightly higher than due to only change of temperature.

**Table 4** Maximum values of the rail displacements and the normal forces in the rail resulting from load combinations, $p$ = 15 N/mm on the loaded section

| | Load combination | Effect | Number of load case and position of the beginning of the braking in front of the tunnel | | | | | | |
|---|---|---|---|---|---|---|---|---|---|
| | | | I. 300 m | II. 250 m | III. 200 m | IV. 150 m | V. 100 m | VI. 50 m | VII. 0 m |
| 1. | winter | displacement $e_x$ [mm] | −1.975 | −1.347 | −1.347 | −1.347 | −1.347 | −1.347 | −1.975 |
| 2. | summer | displacement $e_x$ [mm] | 2.707 | 1.802 | 1.802 | 1.802 | 1.802 | 1.802 | 2.707 |
| 3. | braking → | displacement $e_x$ [mm] | 0.417 | 0.417 | 0.417 | 0.417 | 0.417 | 0.417 | 0.417 |
| | | normal force $N$ [kN] | ±28.95 | ±28.95 | ±28.95 | ±28.95 | ±28.95 | ±28.95 | ±28.95 |
| 4. | braking ← | displacement $e_x$ [mm] | −0.417 | −0.417 | −0.417 | −0.417 | −0.417 | −0.417 | −0.417 |
| | | normal force $N$ [kN] | ±28.95 | ±28.95 | ±28.95 | ±28.95 | ±28.95 | ±28.95 | ±28.95 |
| 5. | winter + brake → | displacement $e_x$ [mm] | −1.356 | −0.725 | −0.725 | −0.725 | −0.725 | −0.725 | −1.356 |
| | | normal force $N$ [kN] | 1030.62 | 1030.62 | 1030.62 | 1030.62 | 1030.62 | 1030.33 | 1001.67 |
| 6. | winter + brake ← | displacement $e_x$ [mm] | −3.521 | −3.603 | −3.624 | −3.624 | −3.624 | −3.603 | −3.521 |
| | | normal force $N$ [kN] | 1001.67 | 1001.67 | 1001.67 | 1001.67 | 1001.67 | 1001.67 | 1001.67 |
| 7. | summer + brake → | displacement $e_x$ [mm] | 4.886 | 4.939 | 4.989 | 4.990 | 4.989 | 4.939 | 4.886 |
| | | normal force $N$ [kN] | −777.15 | −777.15 | −777.15 | −777.15 | −777.15 | −777.15 | −777.15 |
| 8. | summer + brake ← | displacement $e_x$ [mm] | 1.887 | 0.998 | 0.998 | 0.998 | 0.998 | 0.998 | 1.877 |
| | | normal force $N$ [kN] | −806.11 | −806.11 | −806.11 | −806.11 | −806.11 | −805.75 | −777.15 |

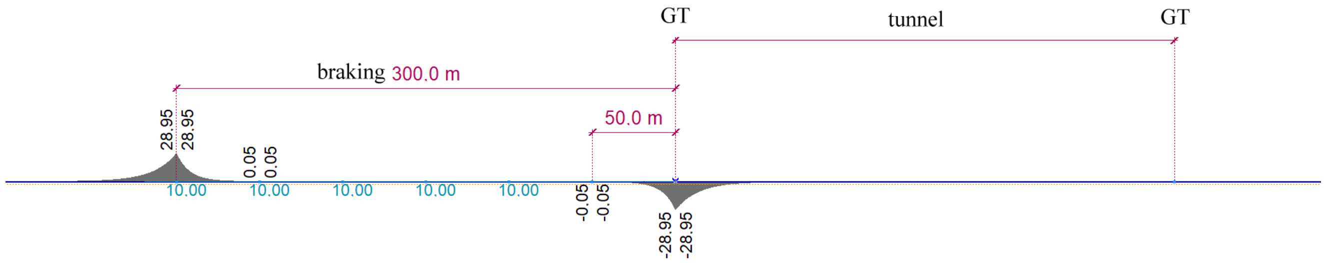


**Fig 17** Normal forces [kN] in the rail due to right braking (→) starting 300 m in front of the gate of the tunnel, $p$ = 15 N/mm

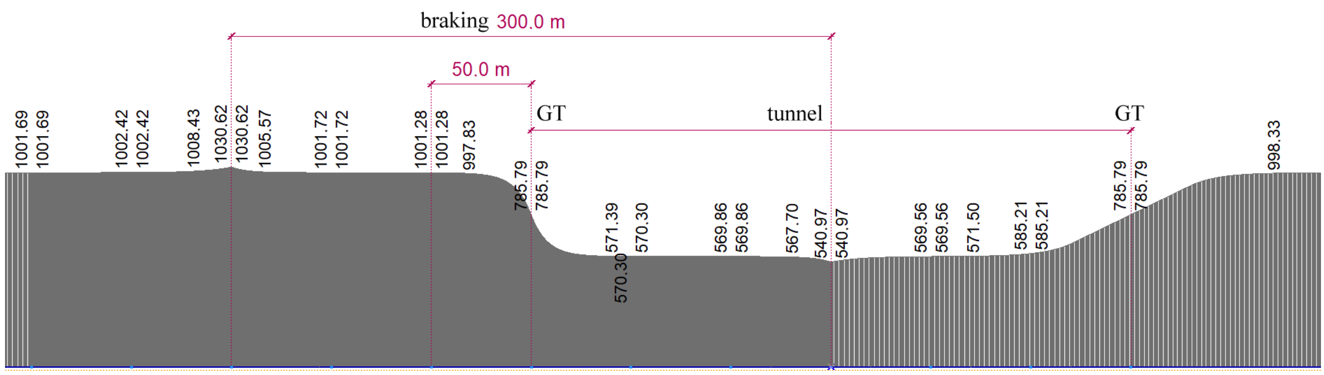


**Fig 18** Normal forces [kN] in the rail due to winter temperature and right (→) braking starting 150 m in front of the gate of the tunnel, $p$ = 15 N/mm

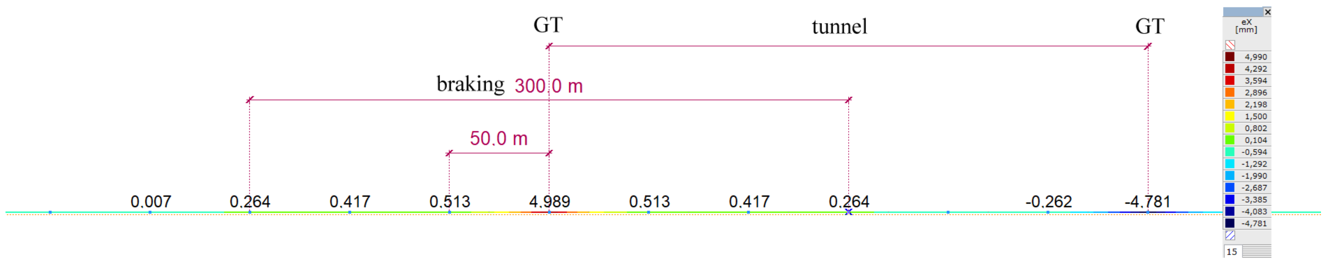


**Fig 19** Longitudinal displacement [mm] of the rail due to summer temperature and right (→) braking starting at 150 m in front of the tunnel, $p$ = 15 N/mm

## 8 Conclusions

The conclusions of the computations presented in this paper can be summarized for the temperature conditions of Case "A" in the following paragraphs:

With the assumption that the longitudinal resistance of the ballast is $p$ = 7 N/mm for the 300 m long section loaded with the braking force:

- The maximum rail displacement is 81.520 mm, which is obtained from the combined effect of the temperature change and the braking force by non-linear calculation, based on the calculation results obtained from a model that also takes into account the effect of the vertical load of the trains.
- The maximum rail displacement due to summer temperature change alone is 3.505 mm and 36.271 mm due to braking alone, on the loaded model.
- The combined effect of the two loads results in 81.520 – 3.505 = 78.015 mm more displacement than the thermal load alone.
- With one or two exceptions, the displacements due to temperature changes occur on the unloaded track, which was calculated to be 4.781 mm (Table 1).
- If this value is added to the value of 78.015 mm mentioned above, the total displacement of the rail is 4.781 + 78.015 = 82.796 mm. This value represents the combined effect of thermal expansion of the unloaded rail and the displacement of the loaded rail due to the braking with increased stiffness and resistance.

With the assumption that the longitudinal resistance of the ballast is $p$ = 10 N/mm for the 300 m long section loaded with the braking force:

- The maximum rail displacement is 30.653 mm, which is obtained from the combined effect of the temperature change and the braking force by non-linear calculation, based on the calculation results obtained from a model that also takes into account the effect of the vertical load of the trains.
- The maximum rail displacement due to summer temperature change alone is 2.547 mm and 0.625 mm due to braking alone, on the loaded model.
- The combined effect of the two loads results in 30.653 – 2.547 = 28.106 mm more displacement than the thermal load alone.
- If the value of 28.106 mm is added to the displacement generated by temperature change alone, the total displacement of the rail is 4.781 + 28.106 = 32.887 mm. This value represents the combined effect of thermal expansion of the unloaded rail and the displacement of the loaded rail due to the braking with increased stiffness and resistance.

With the assumption that the longitudinal resistance of the ballast is $p$ = 15 N/mm for the 300 m long section loaded with the braking force:

- The maximum rail displacement is 4.990 mm, which is obtained from the combined effect of the temperature change and the braking force.
- The maximum rail displacement due to summer temperature change alone is 1.802 mm and 0.417 mm due to braking alone, on the loaded model.
- The combined effect of the two loads results in 4.990 – 1.802 = 3.188 mm more displacement than the thermal load alone.
- If the value of 3.188 mm is added to the displacement generated by temperature change alone, the total displacement of the rail is 4.781 + 3.188 = 7.969 mm. This value represents the combined effect of thermal expansion of the unloaded rail and the displacement of the loaded rail due to the braking with increased stiffness and resistance.

## 9 Discussion

Based on the research presented in this paper due to the combined effect of temperature change and braking, the following results are obtained:

- If the longitudinal ballast resistance ($p$ = 7 N/mm) is less than the uniformly distributed braking force, very high longitudinal rail displacements may occur that is 82.796 mm according to the computations. Also very high additional tensile and compressive normal forces will be added to those generated by change of temperature.
- If the longitudinal ballast resistance ($p$ = 10 N/mm) is equal to the uniformly distributed braking force, still high longitudinal rail displacements may occur that is 32.887 mm according to the computations, but considerably lower than in the previous paragraph. The normal forces in the rail will not be significantly higher due to load combinations including braking forces than those due to only change of temperature.
- If the longitudinal ballast resistance ($p$ = 15 N/mm) is considerably higher than the uniformly distributed braking force, the longitudinal displacement of the rail will be 7.969 mm, that is only 3.188 higher than those from purely change of temperature. The normal forces in the rail will not be significantly higher due to load combinations including braking forces than those due to only change of temperature.

Accurate calculation can only be achieved with a model that can vary the longitudinal elasticity and limiting force of the ballast in a function of the vertical load.

As it has already been mentioned in Section 5.3, the possibility of huge displacements of 70 to 80 mm is very rare in reality, although the results simulate a theoretical case what could happen if the braking force is greater than the ballast resistance. On tracks with clean ballast of good quality, well compacted and consolidated, the longitudinal ballast resistance under the load of the trains can be considered to be 30 N/mm [5, 6, 11] that is higher than the braking force of 10 kN/mm per rail. A loaded ballast resistance of less than 10 kN/mm may occur only directly after laying newly constructed ballast or ballast screening, however in such cases a speed restriction of 40 km/h or appropriate restrictions are ordered. By dynamic ballast stabilizing machines and the self-compaction of the ballast under traffic, the ballast resistance increases rapidly up to higher than the braking force of 10 kN/mm. Since the time duration of the ballast resistance of less than the braking force is limited to short time periods directly after construction or maintenance works, this situation does not have too much significance on the life cycle of the track. This could be analysed in a different research and the results published in a separate paper.

In case of good ballast conditions, when there is only temperature change, small longitudinal displacements (<5 mm) occur and their magnitude decreases with decreasing temperature. When there is only braking force, the train pushes the track in front of it and pulls it behind it. The sign of the forces makes this clear. After the braking, when the forces are removed, the backward rearranging takes place, but there will always be some residual displacements or residual stresses in the rails due to the unevenness that always exists in reality, i.e. non-ideal conditions. Another software should be used to model this.

If braking is a typical event in front of the tunnel due to some external circumstance, it will affect the wear of the rails. It is also important to ensure that the clamping force of the rail fastenings and the longitudinal ballast resistance are maintained. These may require additional maintenance. In winter, rail fracture due to increased tensile forces caused by braking can be a problem. In the summer, the compressive forces are increased by braking. However, in case of good ballast conditions, the calculated values are not so high that they would be a problem if the material qualities and maintenance are adequate, so there is no safety concern. There is no point in giving a recommended value as there are so many influencing factors. However, it is possible to require numerical verification of the phenomenon in design cases.

This paper highlights the importance of maintaining good and proper ballast properties in tracks in order to conform with the combined effects of change of temperature and braking loads. If they are fulfilled, the maximum longitudinal displacements are below 10 mm, as shown in this paper.

## Nomenclature

| | |
|---|---|
| $p$ (N/mm): | longitudinal ballast resistance, |
| $E$ (N/mm$^2$): | elasticity modulus of the rail, |
| $A$ (mm$^2$): | total cross-sectional area of the rail, |
| $\alpha$ (1/°C): | linear expansion coefficient of rail steel, |
| $\Delta T$ (°C): | change of temperature, |
| $e$ (mm): | displacement of the rail, |
| $e_x$ (mm): | axial displacement of the rail, |
| $N$: | normal force in the rail, |
| $\tau$, $\tau(e_b - e)$: | axial shear resistance, depending on the difference of the displacements, |
| $EA$: | axial normal stiffness of the rail, |
| $\alpha\ \Delta T$: | temperature strain of the rail, |
| GT: | gate of tunnel. |

## References


[1] MÁV Zrt. "D.12/H. Utasítás: Hézagnélküli felépítmény építése, karbantartása és felügyelete" (Instructions of MÁV Zrt D.12.H of Hungarian State Railways, of construction and maintenance of CWR tracks), [pdf] KÖZDOK, Budapest, 2009. (in Hungarian)

[2] Nemesdy, E. "Vasúti Felépítmény" (Railway Superstructure), Tankönyvkiadó, Budapest, 1966. (in Hungarian)

[3] Nemesdy, E. "A hézagnélküli vasúti pályák gátolt dilatációjának pontos és közelítő számítása, valamint a sínvégek illesztésének kialakítása" (Accurate and approximative calculation of constrained dilatation of continuously welded rail tracks, and formation of rail joints), Scientific proceedings of the Technical University of Construction and Transport, Budapest, 5(2–5), 1960. (in Hungarian)

[4] CEN "EN 1991-2:2003 Eurocode 1: Actions on structures - Part 2: Traffic loads on bridges", European Committee for Standardization, Brussels, Belgium, 2003.

[5] Freystein, H., Muncke, M., Schollmeier, P. "Handbuch Entwerfen von Bahnanlagen" (Manual for designing railroad systems), Eurailpress in DVV Media Group, 2005. ISBN: 3-7771-0333-0 (in German)

[6] International Union of Railways "Track - bridge Interaction. Recommendations for calculations", [pdf] UIC, Paris, France, 2001.

[7] Esveld, C. "Modern Railway Track", MRT Production, 2014. ISBN: 978-1-326-05172-3

[8] Mirkovic, N., Brajovic, L., Popovic, Z., Todorovic, G., Lazarevic, L., Petrovic, M. "Determination of temperature stresses in CWR based on measured rail surface temperatures", Construction and Building Materials, 284, 122713, 2021. https://doi.org/10.1016/j.conbuildmat.2021.122713

[9] Chapman, L., Thornes, J. E., White, S. P. "Thermal imaging of railways to identify track sections prone to buckling", Proceedings of the Institution of Mechanical Engineers, Part F: Journal of Rail and Rapid Transit, 220(3), pp. 317–327, 2006. https://doi.org/10.1243/09544097JRRT73

[10] Ryan, M. "Rail temperature measurement study", AEA Technology Rail, Derby, UK, 2005.

[11] Popović, Z., Mirković, N., Brajović, L., Rakić, D., Lazarević, L., Petričević, S. "Temperature stresses in CWR - experience of Serbian Railways", In: Popovic, Z., Manakov, A., Breskich, V. (eds.) VIII International Scientific Siberian Transport Forum, Novosibirsk, Russia, 2020, pp. 825–833. ISBN: 978-3-030-37916-2 https://doi.org/10.1007/978-3-030-37916-2_81

[12] Kupfer, R. "Auswirkungen von Beschleunigungs- und Bremskräften auf die Längsbewegungen des Gleisrostes" (Effects of accelerating and braking forces on longitudinal movements of the track structure), PhD Dissertation, Technische Universität München (Technical University of Munich), 2004. Available at: https://mediatum.ub.tum.de/?id=601061 (in German)

[13] Liu, S., Fu, J., Yang, J., Feng, H. "Numerical Simulation of Temperature Effects on Mechanical Behavior of the Railway Tunnel in Tibet", KSCE Journal of Civil Engineering, 24(12), pp. 3875–3883, 2020. https://doi.org/10.1007/s12205-020-1893-1

[14] Peltier, M., Rotta Loria, A., Lepage, L., Garin, E., Laloui, L. "Numerical investigation of the convection heat transfer driven by airflows in underground tunnels", Applied Thermal Engineering, 159, 113844, 2019. https://doi.org/10.1016/j.applthermaleng.2019.113844

[15] Fazilova, Z., Loktev, A., Shapran, V. "Simulating of the heat conduction processes and their impact on the stress-strain state of the continuously welded rail structure", IOP Conference Series: Materials Science and Engineering, 919, 052029, 2020. https://dx.doi.org/10.1088/1757-899X/919/5/052029

[16] Davies, G., Boot-Handford, N., Curry, D., Dennis, W., Ajileye, A., Revesz, A., Maidment, G. "Combining cooling of underground railways with heat recovery and reuse", Sustainable Cities and Society, 45, pp. 543–552, 2019. https://doi.org/10.1016/j.scs.2018.11.045

[17] Tinti, F., Boldini, D., Ferrari, M., Lanconelli, M., Kasmaee, S., Bruno, R., Egger, H., Voza, A., Zurlo, R. "Exploitation of geothermal energy using tunnel lining technology in a mountain environment. A feasibility study for the Brenner Base tunnel – BBT", Tunnelling and Underground Space Technology, 70, pp. 182–203, 2017. https://doi.org/10.1016/j.tust.2017.07.011

[18] Piccinini, L., Vincenzi, V. "Impacts of a railway tunnel on the streams baseflow verifed by means of numerical modelling", Acque Sotteranee Italian Journal of Groundwater, 10(1), pp. 123–134, 2010. https://doi.org/10.7343/as-2021-503

[19] Sanchis, I., Franco, R., Zuriaga, P., Fernández, P. "Risk of increasing temperature due to climate change on operation of the Spanish rail network", Transportation Research Procedia, 45, pp. 5–12, 2020. https://doi.org/10.1016/j.trpro.2020.02.056

[20] Mulholland, E., Feyen, L. "Increased risk of extreme heat to European roads and railways with global warming", Climate Risk Management, 34, 100365, 2021. https://doi.org/10.1016/j.crm.2021.100365

[21] Zakeri, J., Yousefian, K. "Experimental investigation into the longitudinal resistance of ballasted railway track", Proceedings of the Institution of Mechanical Engineers, Part F: Journal of Rail and Rapid Transit, 235(8), pp. 969–235, 2020. https://doi.org/10.1177/0954409720975522

[22] De Iorio, A., Grasso, M., Penta, F., Pucillo, G. P., Rossi, S., Testa, M. "On the ballast–sleeper interaction in the longitudinal and lateral directions", Proceedings of the Institution of Mechanical Engineers, Part F: Journal of Rail and Rapid Transit, 232(2), pp. 620–631, 2018. https://doi.org/10.1177/0954409716682629

[23] Dersch, M. S., Potvin, M., Lima, A. de O., Edwards, J. R. "Effect of Critical Factors Influencing Longitudinal Track Resistance Leveraging Laboratory Track Panel Pull Test Experimentation", Transportation Research Record, 2677(8), pp. 54–65, 2023. https://doi.org/10.1177/03611981231155420

[24] Dersch, M. S., Potvin, M., de O. Lima, A., Edwards, J. R. "Effect of Critical Factors Influencing Longitudinal Track Resistance Leveraging Field Experimentation", Transportation Research Record, 2678(5), pp. 102–111, 2024. https://doi.org/10.1177/ 03611981231187641

[25] Potvin, M., Dersch, M., Edwards, J. R., Lima, A. de O. "Review of Critical Factors Influencing Longitudinal Track Resistance", Transportation Research Record, 2677(7), pp. 558–569, 2023. https://doi.org/10.1177/03611981231155170

[26] Nobakht, S., Zakeri J., Safizadeh, A. "Investigation on longitudinal resistance of the ballasted railway track under vertical load", Construction and Building Materials, 317, 126074, 2022. https://doi.org/10.1016/j.conbuildmat.2021.126074

[27] Safizadeh, A., Zakeri J., Nobakht, S. "Laboratory investigation on contribution of fastening system and sleeper in longitudinal resistance of ballasted railway tracks", Road Materials and Pavement Design, 24(7), pp. 1712–1727, 2022. https://doi.org/10.1080/14680629.2022.2096104

[28] Alizadeh, M., Imani, M., Zakeri, J. A. "Laboratory and numerical investigation on the longitudinal resistance of ballasted railway tracks with steel sleepers", Construction and Building Materials, 402, 132670, 2023. https://doi.org/10.1016/j.conbuildmat.2023.132670

[29] Mohammadzadeh, S., Esmaeili, M., Khatibi, F. "A new field investigation on the lateral and longitudinal resistance of ballasted track", Proceedings of the Institution of Mechanical Engineers, Part F: Journal of Rail and Rapid Transit, 232(8), pp. 2138–2148, 2018. https://doi.org/10.1177/0954409718764190

[30] Sun, F., Hoult, N., Butler, L. J., Zhang, M. "Field monitoring and prediction of the thermal response of an in-service curved continuous welded rail using distributed fiber optic strain measurements", Journal of Civil Structural Health Monitoring, 2024. https://doi.org/10.1007/s13349-024-00869-8

[31] Liu, G., Liu, H., Wei, A., Xiao, J., Wang, P., Li, S. "A new device for stress monitoring in continuously welded rails using bi-directional strain method", Journal of Modern Transportation, 26(3), pp. 179–188, 2018. https://doi.org/10.1007/s40534-018-0164-z

[32] Ahmad, S. S., Mandal, N. K., Chattopadhyay, G., Powell, J. "Development of a unified railway track stability management tool to enhance track safety", Proceedings of the Institution of Mechanical Engineers, Part F: Journal of Rail and Rapid Transit, 227(5), pp. 493–516, 2013. https://doi.org/10.1177/0954409713501490

[33] Skarova, A., Harkness, J., Keillor, M., Milne, D., Powrie, W. "Review of factors affecting stress-free temperature in the continuous welded rail track", Energy Reports, 8(11), pp. 107–113, 2022. https://doi.org/10.1016/j.egyr.2022.11.151

[34] Shi, C., Zhou, Y., Xu, L., Zhang, X., Guo, Y. "A critical review on the vertical stiffness irregularity of railway ballasted track", Construction and Building Materials, 400, 132715, 2023. https://doi.org/10.1016/j.conbuildmat.2023.132715

[35] Javaid, O., Choi, D.-H. "Effect of Track Irregularities on the Response of Two-Way Railway Tracks", Applied Sciences, 10(1), 11, 2020. https://doi.org/10.3390/app10010011

[36] Tong, Y., Liu, G., Yousefian, K., Jing, G. "Track Vertical Stiffness – Value, Measurement Methods, Effective Parameters and Challenges: A review", Transportation Geotechnics, 37, 100833, 2022. https://doi.org/10.1016/j.trgeo.2022.100833

[37] Musazay, J. A., Zarembski, A. M., Palese, J. W. "Determining track-induced lateral thermal expansion forces on a curved railway track", Proceedings of the Institution of Mechanical Engineers, Part F: Journal of Rail and Rapid Transit, 236(1) pp. 3–14. 2022. https://doi.org/10.1177/0954409721995318

[38] Nazmul, H. "Lateral Stability of a Ballasted Curved Track", Journal of Transportation Engineering, Part A: Systems, 146(11), 06020001, 2020. https://doi.org/10.1061/JTEPBS.0000450

[39] Jing, G. Q., Aela, P., Fu, H., Esmaeili, M. "Numerical and Experimental Analysis of Lateral Resistance of Biblock Sleeper on Ballasted Tracks", International Journal of Geomechanics, 20(6), 04020051, 2020.
https://doi.org/10.1061/(ASCE)GM.1943-5622.0001689

[40] Esmaeili, M., Zakeri, J. A., Babaei, M. "Laboratory and field investigation of the effect of geogrid-reinforced ballast on railway track lateral resistance", Geotextiles and Geomembranes, 45(2), pp. 23–33, 2017.
https://doi.org/10.1016/j.geotexmem.2016.11.003

[41] Fu, J., Zhao, N., Qu, Y., Yang, J., Wang, S. "Effects of twin tunnel undercrossing excavation on the operational high speed railway tunnel with ballastless track", Tunnelling and Underground Space Technology, 124, 104470, 2022.
https://doi.org/10.1016/j.tust.2022.104470

[42] Li, Z., Huang, W., Xu, Z., Tang, X., Wang, M., Yu, L., Li, Z. "Analysis of the Mechanical Characteristics of Different Track Bed Types in Heavy-Haul Railway Tunnels", Mathematical Problems in Engineering, 2021(1), 5527073, 2021.
https://doi.org/10.1155/2021/ 5527073

[43] Fischer, S., Harangozó, D., Németh, D., Kocsis, B., Sysyn, M., Kurhan, D., Brautigam, A. "Investigation of heat-affected zones of thermite rail weldings", Facta Universitatis, Series: Mechanical Engineering, 22(4), pp. 689–710, 2023.
https://doi.org/10.22190/FUME221217008F

[44] Neridu, S., Pasupuleti, V. D. K., Kalapatapu, P. "Analysis of rail structure interaction in continuous welded rails on railway bridges: a parametric analysis", Innovative Infrastructure Solutions, 9(10), 367, 2024.
https://doi.org/10.1007/s41062-024-01687-z

[45] Mubarack, C. K. A., Upadhyay, A. "Effect of Braking Load on Longitudinal Forces in Continuous Welded Rail Considering the Presence of Bridge", In: Madhavan, M., Davidson, J. S., Shanmugam, N. E. (eds.) Proceedings of the Indian Structural Steel Conference 2020 (Vol. 2), 2023, pp. 499–507. ISBN: 978-981-19-9393-0
https://doi.org/10.1007/978-981-19-9394-7_40

[46] CEN "EN 13146-1:2019, European Standard, Railway applications, Track, Test methods for fastening systems, Part 1, Determination of longitudinal rail restraint", European Committee for Standardization, Brussels, Belgium, 2019.

[47] Papp, H., Liegner, N. "Investigation of internal forces in the rail due to the interaction of CWR tracks and steel bridges with ballasted track superstructure", Pollack Periodica, 11(2), pp. 65–74, 2016.
https://doi.org/10.1556/606.2016.11.2.6

[48] Liegner, N., Kormos, G., Papp, H. "Solutions of omitting rail expansion joints in case of steel railway bridges with wooden sleepers", Periodica Polytechnica Civil Engineering, 59(4), pp. 495–502, 2015.
https://doi.org/10.3311/PPci.8169

[49] Liegner, N. "Alagutak kapuzatainál kialakuló síndilatációs mozgások" (Rail dilatation movements at gates of tunnels), Sínek Világa, 2021(4–5) pp. 54–59. Available at: https://www.sinekvilaga.hu/alagutak-kapuzatanal-kialakulo-sindilatacios-mozgasok (in Hungarian)